Reviewer #1:

Review of the manuscript titled: Impacts of Secondary Ice Production on the Microphysics and Dynamics of Deep Convective Clouds in Different Environments, by Waman et al.

Reviewer: This study investigates the impact of incorporating four SIP processes, rime splintering (Hallett–Mossop process, HM), fragmentation during raindrop freezing (RDF), ice–ice collision breakup (IIC), and sublimational breakup (SBF), into NWP simulations using the ICON model with an advanced two-moment microphysical scheme. Four case studies were selected, including three continental and one maritime DCC events.

Comparisons with in situ and satellite observations indicate that the inclusion of SIP processes generally improves the simulation results. Further analysis shows that, relative to simulations without SIP, the inclusion of SIP reduces supercooled liquid water, increases IWC and INC, and enhances both total latent heating and net cloud radiative heating in the mixed-phase region. An increase in cloud-top height is also found. The impact on precipitation is limited for the continental cases, while a positive (increasing) effect is found for the maritime case. Two parameterizations of the RDF process were tested and produced fairly similar results. The influence of the SBF process is found to be negligible.

Overall, the findings provide a valuable contribution to the understanding of SIP in deep convective systems. The manuscript is clearly written and the results are well presented. I offer several suggestions below to further strengthen the study.

Response: We thank the reviewer for their efforts and time in reviewing the manuscript. We hope that the arguments presented by the reviewers will help us to improve the quality of the manuscript. Below are the point-to-point responses to the reviewer's comments.

We would like to draw the reviewer's attention to several important changes in the model setup adopted in the revised analysis.

1. We re-performed both SULL18 and PHIL18 simulations for all deep convective cloud (DCC) cases using an updated treatment of the rime fraction in secondary ice production (SIP) during ice-ice collisions (IIC). In contrast to the previous fixed rime-fraction (0.4) assumption, the revised simulations use a particle size-dependent rime-fraction parameterization following Martanda et al. (2025, Table 2 therein).

2. In all simulated DCCs, together with other SIP processes, fragmentation in freezing raindrop (RDF) using the Phillips et al. (2018, PHIL18) scheme shows a better agreement with observed threshold ice number concentrations (INCs) than the Sullivan et al. (2018; SULL18) RDF scheme. Therefore, the revised **control simulations** use PHIL18 RDF scheme.

3. Our revised analysis of INP concentrations indicates that the Hande et al. (2015) treatment of immersion-freezing INP activation underestimates the observed INP concentrations over the selected study regions. Accordingly, in the revised simulations, the immersion-freezing INP activation of Hande et al. (2015) was scaled to match the

observed INP concentrations for each simulated case. This INP scaling was applied consistently to both the "control (PHIL18)", "SULL18" and "No-SIP" simulations.

Based on these updates, the revised manuscript redefines the control simulations using the variable rime-fraction approach together with RDF from PHIL18, while all simulations additionally include the revised INP scaling. All subsequent analyses and comparisons are presented based on these updated simulations.

Additionally, during the validation of the filtered INC for the simulated DCMEX convection, the observed INC measured by the 2DS probe had previously been plotted using incorrect units (cm^{-3} due to a labeling error, whereas the data were intended to be presented in L^{-1}. This has now been corrected, and the observed INC is consistently shown in L^{-1}) throughout the revised manuscript, including Fig. 7f and Figs. S2d, S3b, and S4(d–i) in the supplement.

In the earlier version of the manuscript, the process rates were incorrectly reported in units of kg^{-1} s^{-1}, whereas the analysis was actually performed using units of kg^{-1}. In the revised manuscript, this issue has been corrected, and the process rates are now consistently reported in the appropriate units of kg^{-1} s^{-1}.

A detailed description of these revisions is provided below. Please note that we have marked the reviewer's comments in **red** and corresponding responses from the authors are in **black**.

General:

Reviewer: ORCESTRA case: there should be remote sensing data available from this campaign (e.g., airborne radar reflectivity). It would significantly strengthen the study if these campaign observations could be incorporated into the analysis. Otherwise, the rationale for selecting this specific case is not entirely clear, as in principle any case with an EarthCARE overpass could have been chosen. Please clarify the scientific motivation for focusing on the ORCESTRA event. In addition, the manuscript states that the CPR reflectivity appears to be biased low. This claim could potentially be evaluated by comparison with available airborne radar reflectivity measurements. Such a comparison would provide stronger support for this conclusion.

Response: We thank the reviewer for this constructive suggestion. We address the two parts of this comment separately.

Scientific motivation for the ORCESTRA case: The ORCESTRA case (03 September 2024) in this study is selected for three main reasons. 1) It is the only marine deep convective case in our study, providing an essential thermodynamic contrast to the three selected continental cases (CAIPEEX, DCMEX, MC3E) and allowing us to assess whether SIP impacts on cloud microphysics and dynamics differ between marine and continental environments. 2) The EarthCARE overpass on 3 September 2024 coincided with active deep convection over the tropical Atlantic, providing more advanced satellite observations of microphysical properties from EarthCARE that are not available from ground-based or airborne platforms alone. 3) From our recent analysis, simultaneous shipborne Cloudnet retrievals of LWC and IWC from the Research Vehicle (RV) Meteor (BOWTIE campaign) provided independent observational

constraints on the microphysical properties of the same convective system, as shown in Figs. 9 (b, c) of the revised manuscript. These combined observational constraints motivated the selection of this specific case. We have added a clarifying sentence to the manuscript at the relevant location.

The text in the revised manuscript now reads as (lines 121-123):
"As this study aims to assess the impacts of SIP on the microphysical and dynamical properties of DCCs in contrasting environments, the ORCESTRA case (3 September 2024) is selected as the only marine deep convective case, providing a thermodynamic contrast to the three continental cases (CAIPEEX, DCMEX, MC3E)."

And at lines 230-232 "An EarthCARE overpass coinciding with active deep convection over the tropical Atlantic on the selected day enabled the use of CPR_CLP_2A microphysical retrievals."

Comparison with airborne radar reflectivity: We thank the reviewer for this suggestion. We checked the availability of airborne radar data from ORCESTRA campaign and found that the High Altitude and Long Range (HALO) research aircraft, equipped with the MIRA cloud radar (Ka-band, 35 GHz, nadir-pointing), was operational at about 13.9 km altitude along the EarthCARE track during 16:05–16:16 UTC on 3 September 2024 (Fig. R1). A side-by-side comparison of CPR (94 GHz, W-band) and HALO-MIRA (35 GHz, Ka-band) radar reflectivity curtains is shown in Fig. R2.

Due to differences in their operating frequency, a direct quantitative comparison between the two instruments is not straightforward. The W-band (94 GHz) and Ka-band (35 GHz) radars have different sensitivities to cloud ice and precipitation, different attenuation characteristics, and different scattering regimes for large hydrometeors. Particularly, W-band radars suffer stronger attenuation in heavy precipitation than Ka-band radars. This is evident in Fig. R2, where the HALO-MIRA ka-band radar shows substantially higher reflectivity (> 20 dBZ) at levels below 4 km that remain largely absent in the EarthCARE CPR observations. This is consistent with stronger W-band attenuation in regions of heavy precipitation below 4 km (Figs. R2 and R3).

We have added the CFAD plots as well as the corresponding explanation in the revised manuscript (lines 446-456, Fig. 9(f-h)) which now reads as;
"For this marine convection, Fig. 9(g-i) shows a CFAD comparison of radar reflectivity from the control simulation (Fig. 9i), EarthCARE-CPR (W-band, Fig. 9g), and the airborne HALO-MIRA cloud radar (Ka-band, Fig. 9h) between 16:05–16:16 UTC. The simulated reflectivity distribution agrees well with HALO-MIRA, with both exhibiting pronounced convective features and median values of about 10 dBZ at most vertical levels. In contrast, EarthCARE-CPR shows a larger occurrence of weak echoes and relatively lower median reflectivity. Although a direct quantitative comparison is not feasible due to differences in radar frequency and attenuation characteristics, the CPR CFAD is consistently shifted toward weaker reflectivity than those of both simulation and HALO-MIRA. This may be attributed to stronger attenuation of the W-band signal in heavy precipitation (Sasikumar et al., 2025). This is particularly evident below 4 km, where HALO-MIRA detects substantially higher echoes

(exceeding 20 dBZ) associated with precipitation, while the EarthCARE-CPR signal is highly attenuated at these levels. As a result, while the simulation and HALO-MIRA exhibit convective features of the selected ORCESTRA convection, the EarthCARE-CPR emphasizes the broader stratiform structure."

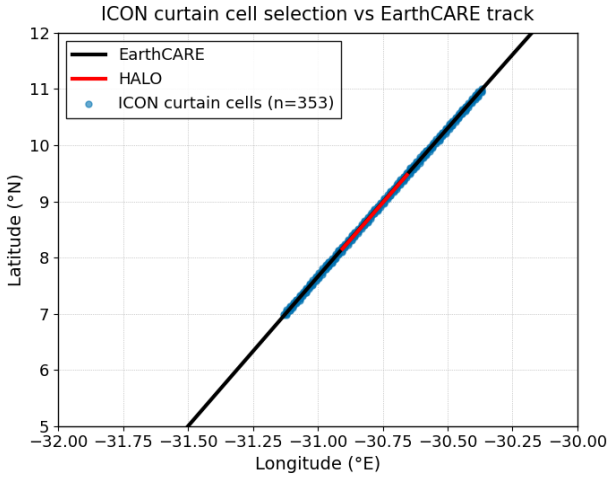

Figure R1: *Spatial collocation of the EarthCARE CPR overpass track (black line), HALO research aircraft flight track (red line), and selected ICON cells (blue dots) along the EarthCARE track during the ORCESTRA case on 3 September 2024 (16:05–16:16 UTC).*

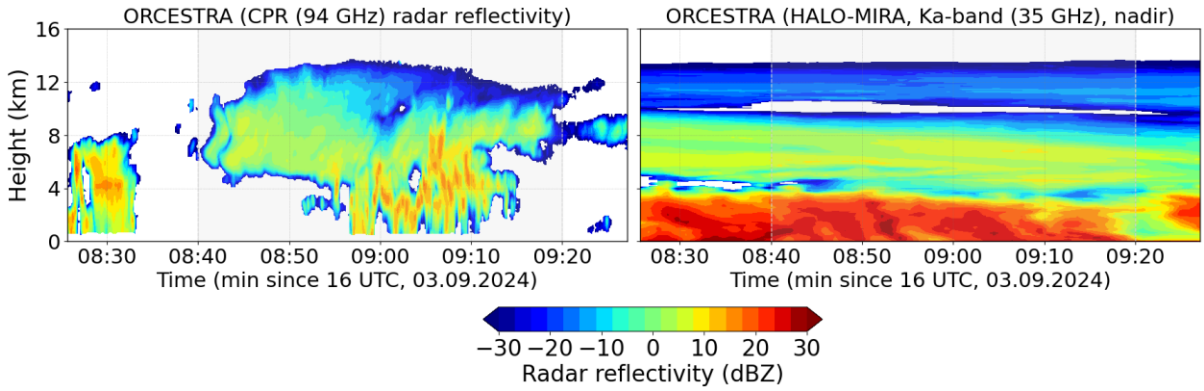

Figure R2: *Time-height cross-sections of radar reflectivity from (a) EarthCARE CPR (94 GHz, W-band) and (b) HALO-MIRA (35 GHz, Ka-band) during the ORCESTRA case on 3 September 2024 (16:05–16:16 UTC). Both instruments were nadir-pointing and spatially collocated along the same flight track (Fig. R1). The higher reflectivity observed by HALO-MIRA below 4 km is consistent with stronger W-band signal attenuation by precipitation in the EarthCARE CPR.*

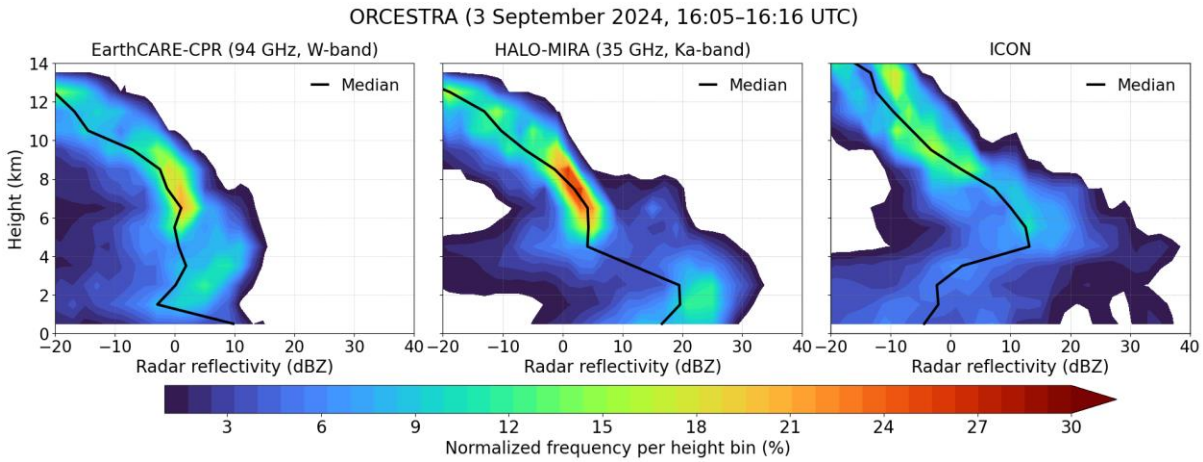

Figure R3: *The contoured frequency by altitude diagram (CFAD) of radar reflectivity from (f) EarthCARE CPR (94 GHz, W-band), (g) HALO-MIRA (35 GHz, Ka-band), and (h) the ICON control simulation for the ORCESTRA case during 16:05–16:16 UTC on 3 September 2024. Both EarthCARE CPR and HALO-MIRA were spatially collocated along the same nadir-pointing track (Fig. R1).*

Reviewer: CAIPEEX case: the exclusion of ice particles with size smaller than 400 µm will have a non-negligible impact on the estimated INC. This needs to be clearly addressed. For example, in the comparison between in situ and simulated INC, a fraction of the simulated INC should be excluded with the same size distributions that the microphysical scheme is used.
Response: We thank the reviewer for raising this important point.

In the revised manuscript, we consistently estimated the ice number concentration for the observational size threshold of ice particles for all simulated DCCs. Figure R4 below shows the simulated ice number concentration for mean particle size larger than 400 µm (N_{400}), consistent with the observational threshold. This is derived by applying the same observational size threshold to the output from control run of CAIPEEX by evaluating the upper incomplete gamma function from D_{thres} = 400 µm to infinity, using the diagnosed shape and scale parameters of the gamma-shaped particle size distribution from the two-moment microphysics scheme. This yields fair comparison of the simulated N_{400} with the observations. From Fig. R4, it is evident that the simulated N_{400} agrees reasonably well with the observations, at both weaker and stronger updraft conditions. The revised figures and discussion in the manuscript reflect this correction (Figs. 6-8).

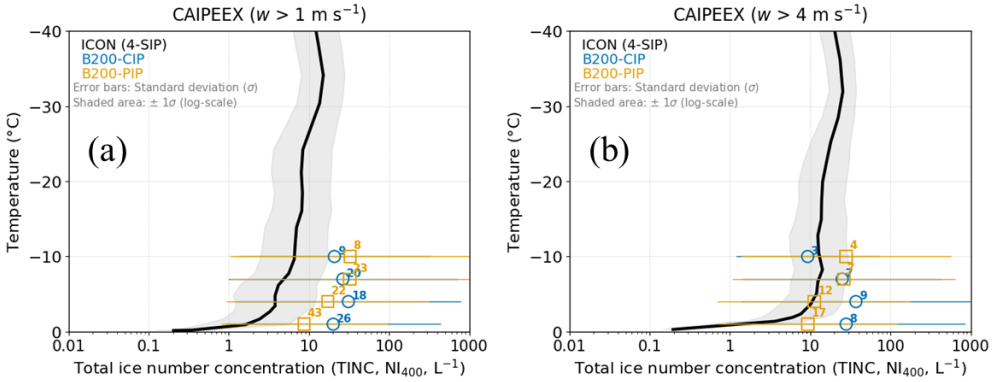

Figure R4: *Comparison of the mean total ice number concentration (TINC) for particles larger than 400 µm (NI_{400}) between the control simulation (black line) and observations from CIP (blue circles) and PIP (orange squares) in the cloudy convective conditions with updrafts exceeding (a) 1 m s^{-1} and (b) 4 m s^{-1}.*

Reviewer: The choice of 1 m/s in the analysis needs to be justified. 1 m/s might be relatively low to isolate the convective updrafts and will probably include more areas affected by wave structures within clouds.

Response: We thank the reviewer for this comment. The initial choice of w > 1 m s^{-1} as the updraft threshold was adopted as a relatively inclusive criterion to retain sufficient data points for better statistical comparison with the aircraft observations (for CAIPEEX, DCMEX, MC3E). However, we agree that these weak updraft regions may include regions influenced by wave structures rather than purely convective updrafts.

To address this concern, we repeated the analysis for stricter updraft thresholds (w > 2 m s^{-1} and > 4 m s^{-1}) for these simulated DCCs, as shown in Figs. R5-R6. The key features of the comparison between the simulated and observed ice number concentrations (N_{ice}) remain qualitatively consistent across all three w-thresholds. This demonstrate that the conclusions are robust regardless of the updraft criterion applied.

We therefore retain w > 1 m s^{-1} in the main manuscript to maximize the observational sample size, given the limited spatial and temporal coverage of the aircraft measurements. The additional figures for w > 2 m s^{-1} and w > 4 m s^{-1} have been included as supplementary material (Fig. S4), and briefly discussed in the revised manuscript (lines 371-374, 396-401, 418).

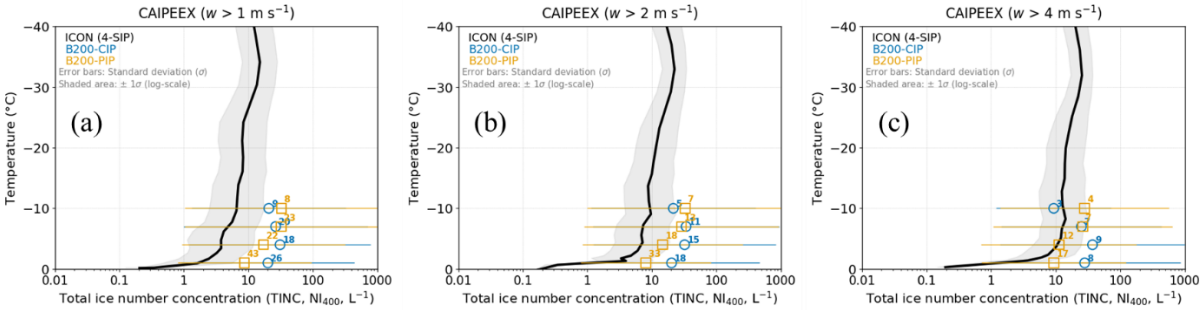

Figure R5: *Comparison of the mean total ice number concentration (TINC) for particles larger than 400 µm (NI_{400}) between the control simulation (black line) and observations from CIP (blue circles)*

and PIP (orange squares) in the cloudy convective conditions of CAIPEEX convection with updrafts exceeding (a) 1 m s^{-1}, (b) 2 m s^{-1}, and (c) 4 m s^{-1}.

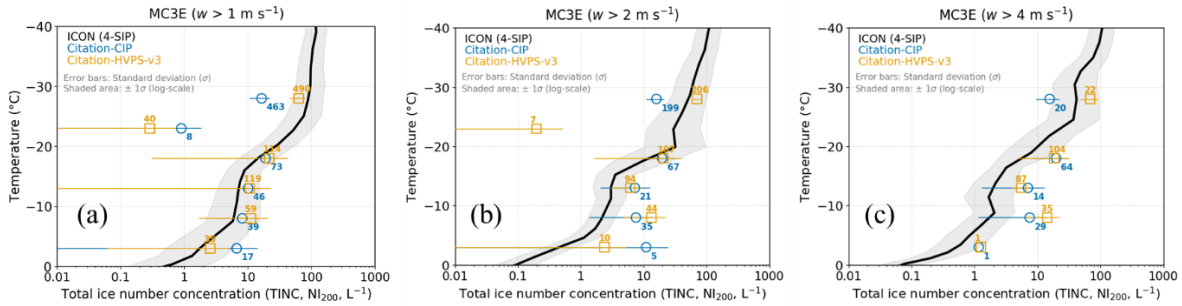

Figure R6: *Comparison of the mean total ice number concentration (TINC) for particles larger than 200 µm (NI$_{200}$) between the control simulation (black line) and observations from CIP (blue circles) and HVPS-v3 (orange squares) probes in the cloudy convective conditions of MC3E convection with updrafts exceeding (a) 1 m s^{-1}, (b) 2 m s^{-1}, and (c) 4 m s^{-1}.*

Technical:

Reviewer: L121-122: repeated phrase to be deleted.
Response: Corrected (lines 140-141 in the revised manuscript).

Reviewer: L123: How many flights were conducted during this campaign? Why choose this specific one? Any other DCCs? Similar for the other three campaigns.
Response: For each campaign, one representative deep convective case was selected for detailed analysis. The CAIPEEX and MC3E cases were chosen to maintain consistency with our previous studies (Waman et al. 2022; Patade et al. 2025), where the same cases were analyzed using different numerical models. The DCMEX and ORCESTRA cases were selected based on: (i) the availability of high-quality microphysical observations from multiple in-situ probes (DCMEX) and EarthCARE satellite, HALO aircraft, and research vessel RV Meteor Cloudnet retrievals (ORCESTRA), (ii) the presence of a well-developed deep convective cloud sampled across a broad temperature range, and (iii) the availability of concurrent meteorological observations to constrain and validate the ICON simulation.

The text in the revised manuscript now reads as (lines 119-123);

"The selection of these cases is based on the intensity of convection, availability of high-quality observations from aircraft, satellite, and ground-based instruments, spanning both stratiform and deep convective regions (especially in CAIPEEX, MC3E, and ORCESTRA)."

Also, providing other specific details, for example number of flights carried for each campaign would considerably extend the manuscript; we therefore refer the reader to the respective campaign papers for further information.

Reviewer: Fig 1a: It will be better if the surface elevation, boarder, etc. could be added in panel (a). Similar for the other three figures.

Response: Corrected in the revised manuscript (Figs. 1-4(a)).

Reviewer: Fig 2c: would it be better to show 2D-S images with higher resolution instead of CIP for this case? Please use the same color map among all the three OAP images. The legend is missing for the panel c as well (same for Fig. 3).
Response: Corrected in the revised manuscript (Figs. 1c, 2c, 3c), with all OAP images are now shown in black and white. For Fig. 2c, we would like to note that the 2D-S images are available for only limited temperature levels.

Reviewer: L186: be careful, EarthCARE is not a radiation budget mission, although it conducts radiative closure assessment. I would suggest: …to study the relationship of cloud, aerosol and radiation.
Response: Thank you for the suggestion. This sentence has been rewritten in the revised manuscript (lines 211-213).

Reviewer: L210: how is CCN simulated in ICON?
Response: In ICON, CCN are not prognostically simulated but are prescribed as a fixed number concentration representative of the assumed aerosol environment. The CCN activation scheme of Segal and Khain (2006) then determines cloud droplet formation using this prescribed CCN concentration, the assumed log-normal aerosol size distribution width, and the vertical velocity at cloud base. The scheme employs regression equations and lookup tables derived from a 2000-bin parcel model and classifies clouds into four aerosol regimes: maritime, continental, intermediate, and polluted continental. Clarification has been added in the revised manuscript (Lines 248-251).

Reviewer: L263: Why the rime fraction is set to 0.4 (for 'snow', I assume)? In Philips et al. 2017, the rime fraction is a variable. This could introduce an uncertainty for the simulation. Should different rime fractions be tested first?
Response: We agree with the reviewer that a fixed rime fraction $\psi = 0.4$ may introduce uncertainty in the ice-ice collision breakup scheme of Phillips et al. (2017). In the revised manuscript, we have replaced the constant rime fraction with a size-dependent step-function formulation following Gautam et al. (2024, their Table 2), which provides physically constrained values of rime fraction as a function of snow particle size, derived from cloud model simulations validated against aircraft observations. This update makes the rime fraction variable within the simulation, consistent with Phillips et al. (2017).

As described earlier, we re-ran all simulations of selected DCCs using the updated rime-fraction formulation and compared the results to simulations with a fixed rime fraction as shown in Figs. R7-R9 below. This comparison reports about 10-20% decrease in total ice number concentrations, especially at subzero temperatures warmer than −20 °C in CAIPEEX, DCMEX and ORCESTRA. In MC3E, the updated formulation of rime fraction shows similarly lower N_{ice} between −7 and −25°C.

It is seen that for ORCESTRA DCCs, modifying ice number concentrations through new rime-fraction approach does not change the mean latent heating over the full simulation period (Fig. R9). However, in these marine DCCs, the temporal evolution of latent heating shows up to

30% stronger heating when the rime fraction is held fixed at 0.4. Furthermore, when comparing a simulation without SIP (No-SIP run) to simulations with both fixed and variable rime fractions, latent heating is more pronounced in the case where the rime fraction is fixed at 0.4 than when it is allowed to vary. Similar changes are reported of continental cases.

This highlights that the choice of rime fraction has a moderate to strong impact on the simulated microphysical and diabatic properties of the clouds. Therefore, in the revised manuscript (line 311), we redefined our PHIL18 and SULL18 simulations using the variable rime-fraction approach (Gautam et al. 2024), and all subsequent analyses are presented with respect to these updated simulations.

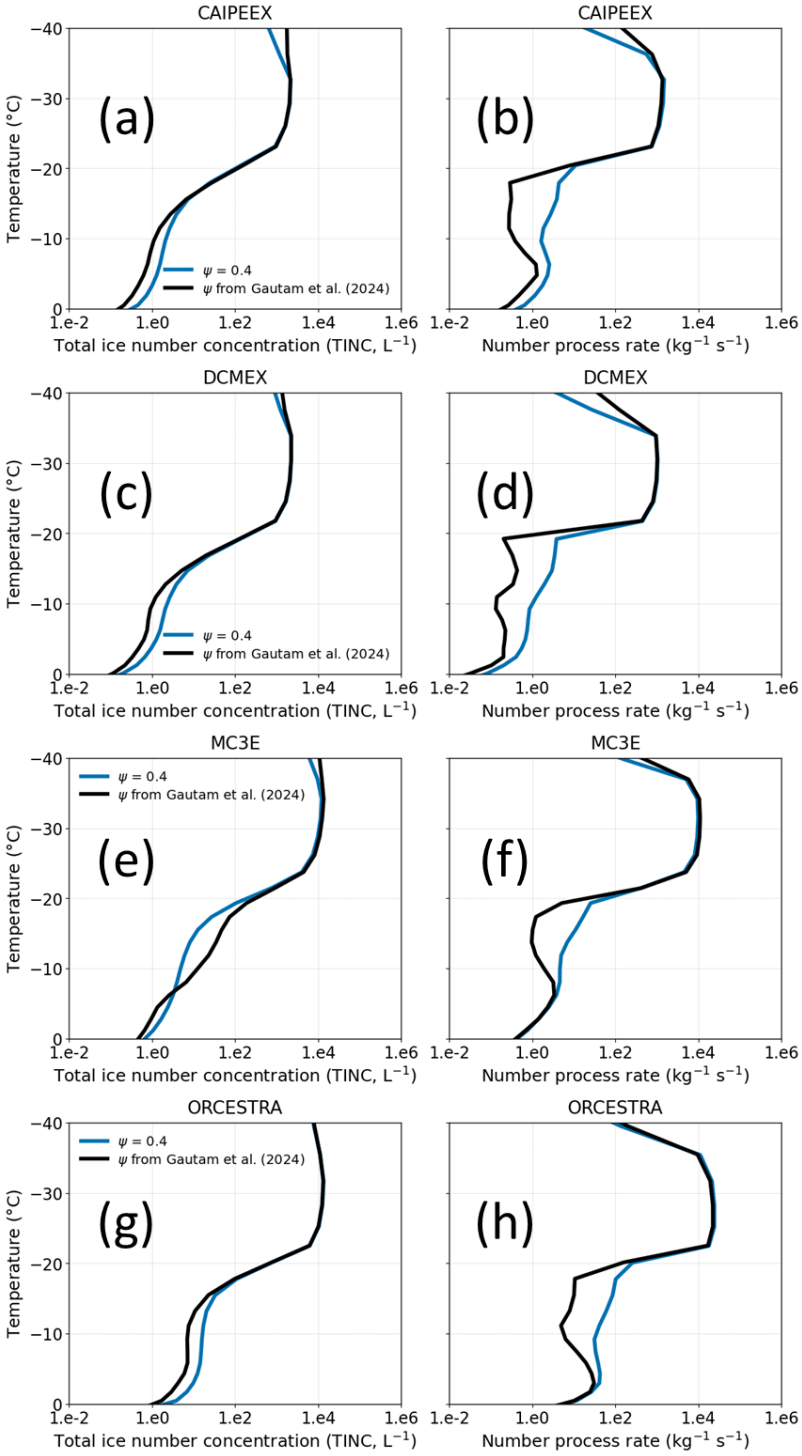

Figure R7: *Profiles of total ice number concentrations (TINC, left panel) and number process rate of SIP in ice-ice collision (right panel) from simulations with (blue line) a fixed rime fraction (ψ), and (red line) rime fraction dependent on particle size (from Gautam et al. 2024)*

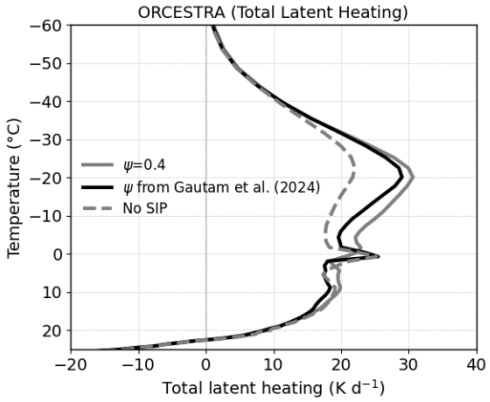

FigureR8: *Profile of mean total latent heating for the marine convection in ORCESTRA, simulated with SIP during ice-ice collision with a fixed rime-fraction (ψ=0.4, solid gray line) and rime-fraction dependent on particle size from Gautam et al. 2024 (solid black line), and without SIP (dashed gray line).*

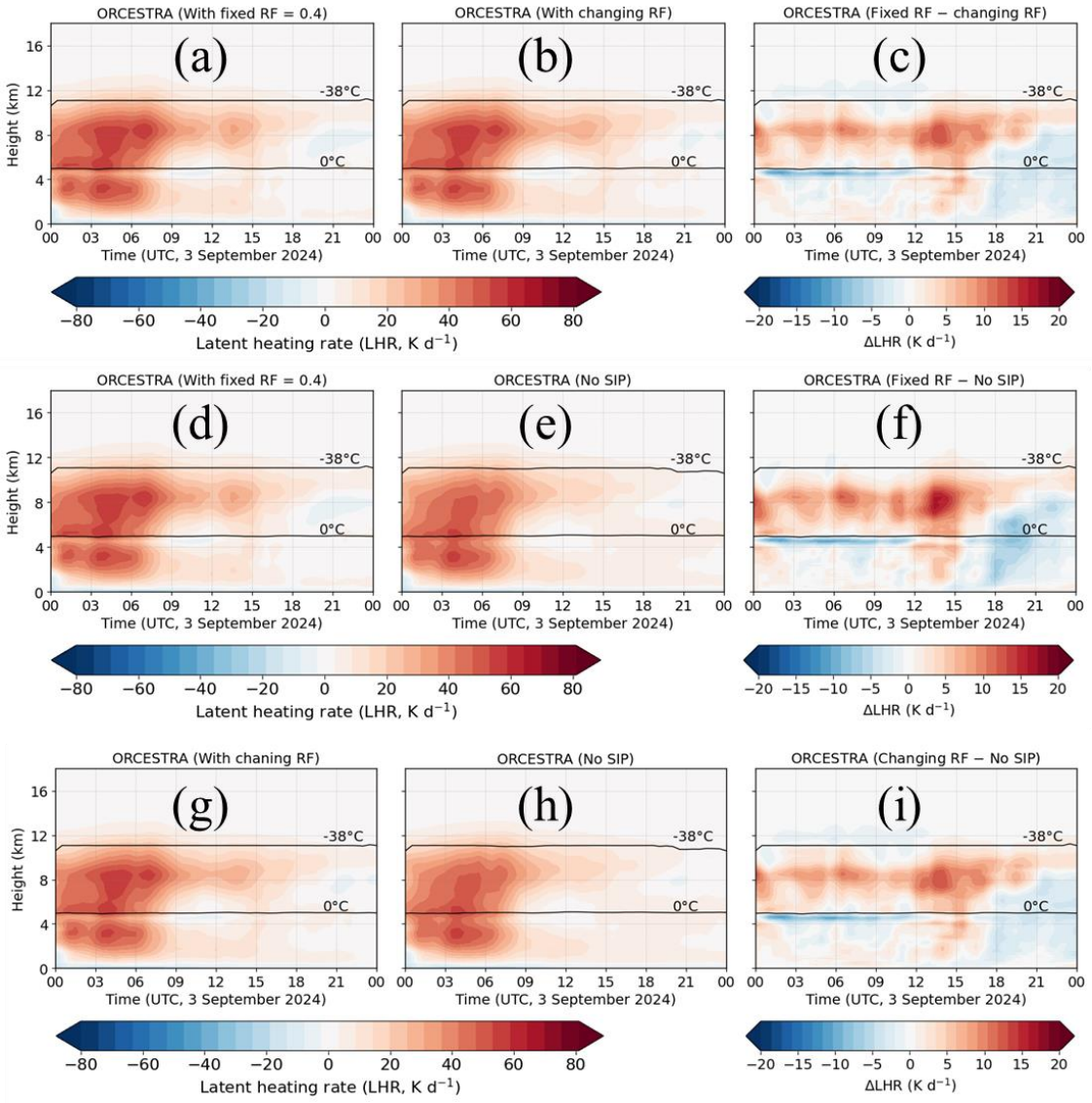

Figure R9: *Time-height profiles of latent heating rate (LHR) for the simulated convection in ORCESTRA, with a fixed and size-dependent rime fraction (ψ) approach for SIP in ice-ice collision. (a, d) LHR with a fixed ψ, (b, g) LHR with ψ from Gautam et al. 2024, (e, h) LHR from No SIP simulation.*

(c) difference in LHR between (a) and (b), (f) change in LHR between fixed ψ and No SIP simulations, and (i) change in LHR between variable ψ and No SIP simulation.

Reviewer: L319: the cloud top can't be seen in Fig. 6e, f.
Response: Corrected in the revised manuscript (Fig. 6g, h).

Reviewer: L319-320: The observed radar reflectivity stayed relatively stable above 5 km. To me the two panels (e, f) are very different, especially for the altitude above the melting layer. It's also better to include a T profile so that we can easily identify the correspondence of T vs. altitude in panel e and f.
Response: We thank the reviewer for noticing this discrepancy. A mean temperature profile has been added as a second y-axis in panels (g) and (h) to visualize temperature levels corresponding to specific altitudes.

Regarding the differences above the melting layer, the broader reflectivity distribution in ICON compared to the quasi-steady reflectivity observed by C-band radar above 5 km likely reflect limitation of the 2-moment bulk microphysics scheme in representing the ice particle size distribution there. C-band radar attenuation in deep convective cores may also contribute to the observed quasi-steady behavior of reflectivity at these levels.

The following text has been added in the revised manuscript (lines 382-384) for more clarification.
"Also, the simulated reflectivity distribution above the freezing level in Fig. 6f is broader than observed. This can be partly attributed to C-band signal attenuation in convective cores and mixed-phase regions (Tian et al. 1997), and limitations of the bulk microphysics scheme in representing the ice particle size distribution at these levels (Ori et al. 2020)."

Reviewer: L327: "simulated IWC four orders of magnitude higher". I believe it's 1 to 2 orders of magnitude instead of 4?
Response: Corrected in the revised manuscript (lines 394).

Reviewer: L329: INC differs by about 4 orders of magnitude rather than 1?
Response: Corrected in the revised manuscript (lines 397).

Reviewer: L343-346: Interestingly that the simulated Z is much higher than the observation, although the pattern looks similar. Any thoughts on the difference? I believe it's important to clarify this difference.
Response: We thank the reviewer for pointing this difference.

The systematically higher simulated reflectivity in ICON compared to the KAZR observations likely reflects two contributing factors. First, the KAZR operational during MC3E is a zenith-pointing ground-based radar that samples a single vertical column. Therefore, KAZR might not have sampled the most intense convective cores if they did not pass directly overhead, while the ICON domain includes all convective cells. Second, the KAZR operates at Ka-band (35 GHz), which is subject to significant signal attenuation in heavy precipitation (Chandra et

al. 2015), particularly in the mixed-phase regions. Since ICON simulates radar-equivalent reflectivity, it does not necessarily include Ka-band attenuation effects present in the Ka-band observations. This would systematically shift the CFAD of simulated reflectivity toward higher values relative to the attenuated KAZR observations.

A clarifying text addressing these differences has been added to the revised manuscript and reads as (lines 422-425);

"However, the higher simulated reflectivity relative to KAZR observations can partly be attributed to Ka-band signal attenuation in heavy precipitation (Chandra et al. 2015) and the single-column sampling limitation of the vertically-pointing KAZR, whose observations are restricted to clouds passing through its narrow vertical sampling volume."

Reviewer: Fig 8c: At some altitudes, there are two distribution bars from HVPS-3. The altitudes might be wrong for one of the two.
Response: We thank the reviewer for their attention to this plotting issue. In the revised manuscript, for all simulated cases, the individual distribution bars have been replaced with mean profiles and their standard deviation, which resolves this plotting issue.

Reviewer: L352: Which EarthCARE product is used here? C-CLD? The product baseline (version) should also be included for reference. This is important as the products are evolving constantly.
Response: We thank the reviewer for this important point. In this study, we used the EarthCARE JAXA CPR Level-2A cloud profile product (CPR_CLP_2A, baseline Bb, processor version 1.1). This information has been added to the manuscript at lines 214–215.

Reviewer: L363: same as above but for radar reflectivity.
Response: The radar reflectivity shown in this figure is also derived from the same EarthCARE JAXA CPR_CLP_2A product (baseline Bb, processor version 1.1), specifically the variable cloud_radar_reflectivity_1km at 1 km resolution. This has been clarified in the manuscript at lines 214-215.

Reviewer: L368-369: "This is chiefly because at higher spatial resolution (1.6 km),". This is not true; CPR product is at ~1 km resolution. To confirm the attenuation of radar signal, it's better to show the quality flag of the CPR products. The 1 m/s threshold should include a lot of regions of mild convection or just regions affected by gravity waves.

Response: We thank the reviewer for this correction. The CPR_CLP_2A product is at 1 km horizontal resolution, comparable to the ICON grid spacing of 1.6 km. The original statement attributing differences in the CFAD to resolution was therefore not justified and has been removed from the manuscript.

Regarding the quality flag, we examined the quality_flag_1km variable from the CPR_CLP_2A product (baseline Bb). This variable contains only fill values (e.g., flag_index 0: [-32767] and the same for flags 1-9) in the current baseline release, indicating it is not yet populated. This was confirmed by re-downloading the same granule, yielding identical results.

As an alternative quality indicator, we provide a supplementary figure (Fig. S4, also Fig. R10) showing the CPR radar reflectivity along the selected EarthCARE curtain over the simulation domain (Fig. R1), retrieved cloud air velocity, and the CPR cloud mask for the EarthCARE overpass on 3 September 2024. The profile-level L2 quality flag is zero across all profiles in this granule, confirming no quality issues were detected at the product level. We expect more comprehensive quality assessment of EarthCARE products in future baseline releases.

Regarding the 1 m/s threshold, we acknowledge the reviewer's concern. Figure R10 below (also supplementary Fig. S4) shows that regions with w > 1 m s^{-1} retrieved by the CPR (Fig. R10, middle panel) coincide predominantly with areas of high radar reflectivity (> 0 dBZ, Fig. R10 left panel), consistent with active convective updrafts rather than gravity-wave-influenced ascent. However, we acknowledge that the 1 m/s threshold cannot fully exclude regions of mild convection or organized stratiform ascent, and this is noted as a limitation of the single EarthCARE overpass available for the selected ORCESTRA case, which precludes a more robust statistical separation of convective and stratiform regimes. This caveat has been added to the manuscript.

The text revised in the updated manuscript is (lines 450-456);

"Although a direct quantitative comparison is not feasible due to differences in radar frequency and attenuation characteristics, the CPR CFAD is consistently shifted toward weaker reflectivity than those of both simulation and HALO-MIRA. This may be attributed to stronger attenuation of the W-band signal in heavy precipitation (Sasikumar et al., 2025). As a result, while simulation and HALO-MIRA exhibit convective features of the selected ORCESTRA convection, CPR preferentially emphasize the broader stratiform structure."

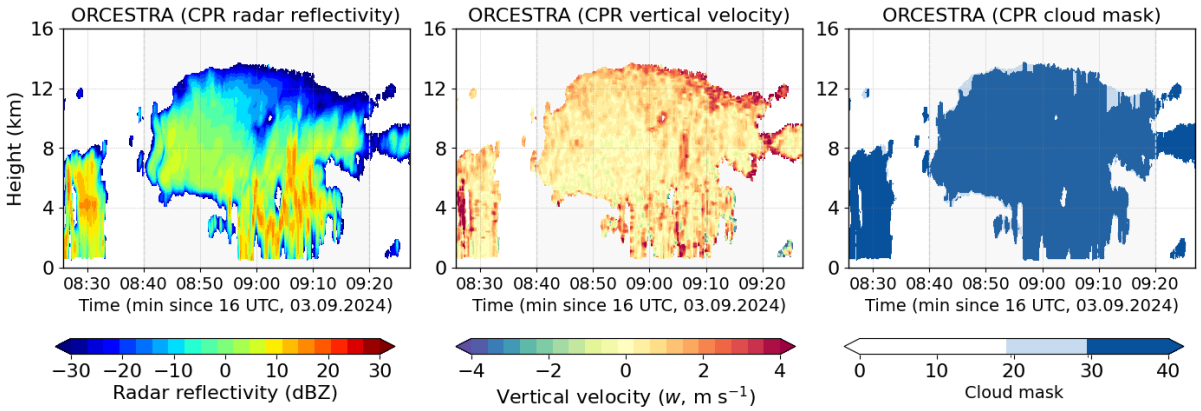

Figure R10: *Time-height profiles of (a) radar reflectivity, (b) cloud air vertical velocity, and (c) cloud mask from the EarthCARE Cloud Profiling Radar (CPR, CPR_CLP_2A, baseline B001) during the ORCESTRA case on 3 September 2024 (16:05-16:16 UTC). The cloud mask values of 20, 30, and 40 represent increasing levels of cloud detection confidence. The quality flag variable in the current product baseline is not yet populated.*

Reviewer: L376: "In summary, ICON adequately reproduces…" might be an overstatement. It is clear though that with SIP, the simulation results improved.

Response: We thank the reviewer for the suggestion. We have modified the text accordingly in the revised manuscript, which now reads as (lines 457-458): "In summary, including different SIP processes in the simulated DCCs improves the agreement between simulated and observed properties."

Reviewer: L386: RDF represent 1% of the SIP: this depends on which parameterization is used. Lawson et al. will produce higher amounts. Note that those results are based on proposed parameterizations, not the 'truth'. Therefore, the statement should be nuanced.
Response: We agree that the relative contribution of RDF can vary depending on the choice of the existing parameterizations. This is also seen with the process rates analyzed for RDF from PHIL18 and SULL18 in the revised manuscript (Fig. S7). The text in the revised manuscript is modified accordingly to reflect this change (Sec. 3.6, lines 639-646).

Reviewer: Fig 13: the x-label of time is misleading: it says a given day (UTC), but the time in the x-axis spans through different days (12 UTC to 12 UTC of the next day).
Response: We thank the reviewer for this observation. In the revised manuscript (Fig. 13, 16(j-i)), the x-axis label has been corrected to 'Time (UTC, 11–12 May 2011)' to reflect that the time series spans two calendar days.

Reviewer: L184-186: It looks like for the first two continental DCCs, excluding SIP increase latent heating during the early growth phase (blue in c & f), opposite to what was stated here?
Response: We thank the reviewer for this observation. The blue regions in Fig. 16 (c, f), during the early growth phase (in CAIPEEX and DCMEX) is primarily due to enhanced condensational latent heating in the 'No SIP' run. Without SIP, the excess water vapor that would otherwise be consumed by depositional growth of extra ice particles from SIP remains available for condensation, producing higher condensational latent heating compared to the control run.

Reviewer: L513: "which weakens CRH through reduced (to up to 20%) depositional growth of ice particles" to "which weakens CRH through radiative effect of reduced (to up to 20%) depositional growth of ice particles"?
Response: We thank the reviewer for this suggestion. However, the weakening of CRH here is through the microphysical pathway as reduced depositional growth lowers the ice water content, which in turn reduces the diabatic heating from deposition rather than through a radiative effect. We would therefore retain the original phrasing but added a clarifying phrase to make the microphysical mechanism explicit (lines 596-558 in the revised manuscript). It now reads as "which weakens CRH through reduced depositional growth of ice particles (by up to 20%), thereby lowering the diabatic heating associated with the ice phase."

References

Tian, L. and Srivastava, R.C., 1997. Measurement of attenuation at C band in a convective storm by a dual-radar method. *Journal of Atmospheric and Oceanic Technology*, *14*(1), pp.184-196.

Ori, D., Schemann, V., Karrer, M., Dias Neto, J., von Terzi, L., Seifert, A. and Kneifel, S., 2020. Evaluation of ice particle growth in ICON using statistics of multi-frequency Doppler cloud radar observations. *Quarterly Journal of the Royal Meteorological Society*, *146*(733), pp.3830-3849.

Gautam, M., Waman, D., Patade, S., Deshmukh, A., Phillips, V., Jackowicz-Korczynski, M., Paul, F.P., Smith, P. and Bansemer, A., 2024. Fragmentation in Collisions of Snow with Graupel/Hail: New Formulation from Field Observations. Journal of the Atmospheric Sciences, 81(12), pp.2149-2164.

Chandra A, Zhang C, Kollias P, Matrosov S, Szyrmer W. Automated rain rate estimates using the Ka-band ARM zenith radar (KAZR). Atmospheric Measurement Techniques. 2015 Sep 14;8(9):3685-99.